PM-IRRAS Investigation of the Interaction of Serum Albumin and Fibrinogen with a Biomedical-Grade Stainless Steel 316LVM Surface

Marie J. Desroches, Nida Chaudhary, and Sasha Omanovic*

Department of Chemical Engineering, McGill University, Montreal, QC, H3A 2B2, Canada

Received March 12, 2007; Revised Manuscript Received May 1, 2007

Polarization modulation infrared reflection absorption spectroscopy (PM-IRRAS) was applied to investigate the interaction of bovine serum albumin (BSA) and fibrinogen with a biomedical-grade 316LVM stainless steel surface, in terms of the adsorption thermodynamics and adsorption-induced secondary structure changes of the proteins. Highly negative apparent Gibbs energy of adsorption values revealed a spontaneous adsorption of both proteins onto the surface, accompanied by significant changes in their secondary structure. It was determined that, at saturated surface coverages, lateral interactions between the adsorbed BSA molecules induced rather extensive secondary structure changes. Fibrinogen's two coiled coils appeared to undergo negligible secondary structure changes upon adsorption of the protein, while large structural rearrangements of the protein's globular domains occurred upon adsorption. The secondary structure of adsorbed fibrinogen was not influenced by lateral interactions between the adsorbed fibrinogen molecules. PM-IRRAS was deemed to be viable for investigating protein adsorption and for obtaining information on adsorption-induced changes in their secondary structures.

1. Introduction

Protein adsorption at solid−liquid interfaces is a widespread phenomenon encountered across various disciplines. In the field of biomaterials and medical implants, it is widely accepted that one of the initial events that significantly influences biocompatibility is the nearly instantaneous adsorption of proteins from biological fluids onto biomaterial surfaces.[1] This adsorbed protein film may be beneficial for certain biomedical applications where the immobilization of specific proteins and enzymes is necessary or desirable, such as in the case of immunoassays and biosensors. However, for blood-contacting medical devices (including cardiovascular stents, catheters, and heart valves), the complex layer of adsorbed plasma proteins is generally unfavorable and could potentially lead to major complications, including thrombus formation, inflammatory tissue responses, and microbial infections.[2,3]

Two plasma proteins that are of particular interest when studying the biocompatibility of blood-contacting implant devices are serum albumin and fibrinogen. Serum albumin (MW $\sim$ 66.3 kDa, dimensions of $15 \times 3.8 \times 3.8$ nm^3)[4] is the most abundant protein present in plasma (totaling up to 60%) with blood concentrations ranging from 30 to 50 g/L.[5] Its main physiological function involves the transport of free fatty acids, which are otherwise insoluble in plasma, to tissues.[6] The protein's (heart-shaped) globular structure is achieved by the folding of its polypeptide chain (containing 585 amino acid residues) into three α-helical domains[7,8] (Scheme 1). Because of its high concentration, serum albumin arrives first at the implant's surface according to the laws of mass transport, and therefore plays an important role in the initial adsorption of proteins onto biomaterial surfaces.

Scheme 1. Three-Dimensional Model of Serum Albumin Showing a High Content of the α-Helical Secondary Structure[8]

Scheme 2. Three-Dimensional Model and Corresponding Schematic Diagram of Fibrinogen Showing the Protein's Different Domains and Secondary Structures[9]

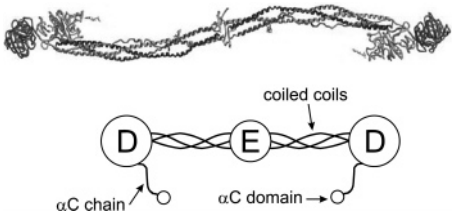

Fibrinogen (MW $\sim$ 340 kDa) is the third primary plasma protein following serum albumin and immunoglobulins, with concentrations typically ranging from 1.5 to 4.0 g/L.[10] It is an elongated, symmetrical dimer (Scheme 2) having approximate dimensions of $47 \times 4.5 \times 4.5$ nm^3, and its distinguishable regions include two hydrophobic outer domains (D domains) connected to a central globular hydrophobic domain (E domain) through two pairs of three nonidentical α-helix coils (Aα, Bβ, and γ chains).[11] In addition, the terminus of the Aα chain forms small globular domains (αC units) that are believed to interact with each other at the central E region of the molecule through their hydrophobic regions.[12] Fibrinogen plays a critical role in the blood coagulation cascade, where the protein's peptide

* Author to whom correspondence should be addressed. Address: Department of Chemical Engineering, McGill University, 3610 University Street, Montreal, QC, H3A 2B2, Canada. Phone: (514) 398-4273. Fax: (514) 398-6678. E-mail: sasha.omanovic@mcgill.ca.

10.1021/bm070289d CCC: $37.00
Published on Web 08/23/2007

Table 1. Chemical Composition of the Biomedical-Grade 316LVM Stainless Steel (weight %)[a]

Fe	Cr	Ni	C	Mo	Mn	S	Si	P	Cu	Sn	Co	N	Nb
bulk	16.57	10.34	0.016	2.13	1.54	0.001	0.54	0.024	0.28	0.009	0.09	0.03	0.01

[a] The data was obtained from the manufacturer (Atlas Stainless Steels) and confirmed by our chemical analysis.

fragments are ultimately cleaved by the enzyme thrombin to yield insoluble fibrin monomers that polymerize into an intricate cross-linking pattern that stabilizes the aggregated platelet plug at the injury site.[13] In addition, fibrinogen is categorized as a cell adhesive protein, and contains the RGD peptide sequence known to bind and activate platelets.[12] Because of these characteristics, fibrinogen adsorption on foreign surfaces has been shown to render otherwise inert materials into thrombogenic surfaces.[14,15]

Since a comprehensive understanding of the mechanisms of protein adsorption is essential for the continuous development of more biocompatible medical devices, the interfacial behavior of proteins has long attracted the interest of researchers. A wide variety of experimental techniques have been applied to study different aspects of protein interaction with solid surfaces, including enzyme-linked immunosorbent assay,[16,17] radiolabeling,[18−20] ellipsometry,[21−24] total internal reflection fluorescence,[25,26] optical waveguide lightmode spectroscopy,[22,27,28] surface plasmon resonance,[29−32] neutron reflectivity,[33,34] electrochemical quartz crystal nanobalance,[35,36] quartz crystal microbalance,[22,37,38] electrochemical impedance spectroscopy (EIS),[39] X-ray photoelectron spectroscopy,[40,41] time-of-flight static secondary ion mass spectroscopy,[42] and IR-based techniques such as attenuated total reflection Fourier transform IR (FTIR),[2,18,43] grazing angle FTIR[5,18] and circular dichroism.[44]

The purpose of this work is to investigate the interaction of two major plasma proteins, bovine serum albumin (BSA) and fibrinogen, with a biomedical-grade 316LVM stainless steel surface by means of the polarization modulation infrared reflection absorption spectroscopy (PM-IRRAS) technique. Aspects of this interaction include the thermodynamics of protein adsorption as well as the possible conformational changes that BSA and fibrinogen undergo upon adsorption to the solid surface. A biomedical-grade 316LVM stainless steel was selected as the substrate since it is a widely used material for certain biomedical applications, particularly for vascular stents. It is also commonly used in a range of other biomedical applications, such as hip prosthesis, screws, external fixations, and so forth. To the best of our knowledge, this is the first report describing the application of the PM-IRRAS technique for investigating the interaction of these two serum proteins with a 316LVM surface. PM-IRRAS offers a number of advantages over other IR techniques, including significantly reduced measurement times, elimination of a background reference scan, virtual elimination of atmospheric water vapor and CO_2 interferences, and high signal-to-noise ratio, thus allowing characterization of organic layers at very low surface concentrations (well below a submonolayer level).

2. Experimental

2.1. Substrates. The investigated material consisted of flat, 316LVM stainless steel (Atlas Stainless Steels, Quebec, Canada) coupons having dimensions ca. 2 × 2 cm. The chemical composition of the stainless steel used in this research, given in Table 1, corresponds to a high-purity austenitic low-carbon, low-sulfur stainless steel. Prior to immersion in the protein solutions, all faces of the coupons were wet-polished with 1500- and 4000-grit gradation emery paper to remove impurities and remnants of previously adsorbed protein. To remove grease and polishing residues, the coupons were then successively placed in a sonication bath for 5 min each in ethanol and acetone, followed by abundant rinsing in deionized water.

Table 2. Frequency Range and Corresponding Secondary Structure Assignments for Fitted Amide I Component Bands Applied for the Conformational Studies of BSA and Fibrinogen Adsorbed onto 316LVM Stainless Steel

wavenumber (cm^{-1})	secondary structure assignment
1615−1639	β-sheet
1648−1659	α-helix
1663−1695	β-turns
1695−	CO_{COOH} stretching for Asp and Glu COOH side chains[a]

[a] Asp: aspartate; Glu: glutamate.

2.2. Protein Adsorption. BSA (Sigma-Aldrich Co., Cat. No. A0281) and fibrinogen (from bovine plasma, Sigma-Aldrich Co., Cat. No. F-8630) were both used as received. Stock solutions of the proteins were prepared by dissolving the appropriate amount of protein into 5 mL of a 0.05 M phosphate-buffered saline (PBS, 0.16 M NaCl) solution at pH 7.4. The PBS solution was previously prepared by first dissolving 0.68 g of anhydrous, monobasic potassium phosphate (KH_2PO_4, Sigma-Aldrich Co., Cat. No. P5379) in 39.1 mL of 0.1 M sodium hydroxide (NaOH, prepared from standard 5 N concentrate; ACP Chemicals, Inc.), followed by dilution with deionized water (Nanopure, resistivity of 18.2 MΩ cm) to yield a final volume of 100 mL. Adsorption of the proteins was performed at room temperature (295 K) by immersing the stainless steel coupons in a separate beaker containing 20 mL of PBS to which aliquots of the stock protein solution were progressively added in order to obtain the desired bulk protein concentration. The coupons were left to equilibrate for 40 min, at which point they were carefully removed and rinsed twice with abundant, clean deionized water. Thorough rinsing of the stainless steel coupons following protein adsorption was essential in order to properly remove nonspecifically adsorbed protein from the steel surface. Following protein adsorption and rinsing, the coupons were dried using a gentle stream of argon.

2.3. PM-IRRAS Measurements. PM-IRRAS spectra were recorded using a Bruker Optics PMA50 external module in conjunction with a TENSOR 27 FT-IR spectrometer. A liquid nitrogen-cooled MCT detector was used in all experiments. The rinsed and dried coupons were mounted in the PMA50's sample holder. The wavelength setting on a Hinds PEM-90 was fixed at 1600 cm^{-1} with a half-wave retardation ($\lambda/2$) of 0.5. The sample was scanned for 5 min with 3 cm^{-1} resolution and an aperture setting of 6 mm, and the resulting absorption spectra were recorded between 400 and 4000 cm^{-1}. The incident beam angle used in all experiments was 85°. Manipulations of the resulting absorption spectra, including baseline corrections and smoothing, were performed using Bruker OPUS Spectroscopy v.5.0 software in interactive mode.

2.4. Amide I Band Fitting Procedure. Analysis of the experimental amide I band was performed using the curve-fitting function of the OPUS software and applying the iterative least-squares Levenberg−Marquardt algorithm. Four underlying component bands were selected for the fitting procedure (Table 2). In addition, Gaussian profiles were specified for each band, based on similar conformational studies in the literature.[5,10,45,46] A fitting procedure was first performed on the Amide I band corresponding to the highest protein concentration. For this initial analysis, the underlying component bands' frequency position, width, and intensity were all allowed to vary from their initial

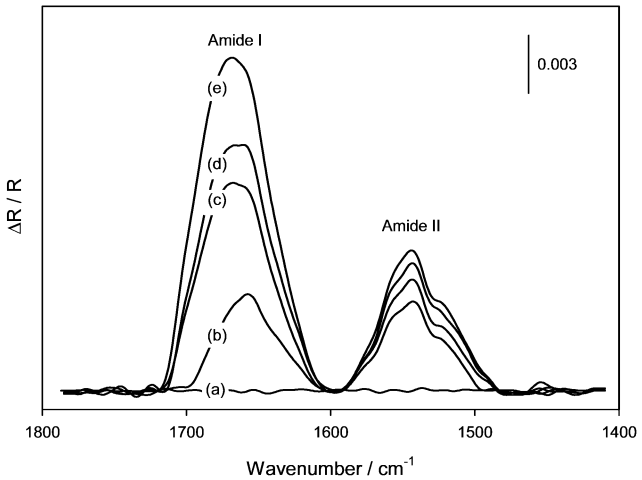

Figure 1. PM-IRRAS spectra of the 316LVM stainless steel surface following immersion in PBS (pH 7.4) solution containing various BSA concentrations: (a) 0 g L^{-1}, (b) 0.05 g L^{-1}, (c) 0.15 g L^{-1}, (d) 0.30 g L^{-1}, and (e) 0.60 g L^{-1}. Temperature = 295 K.

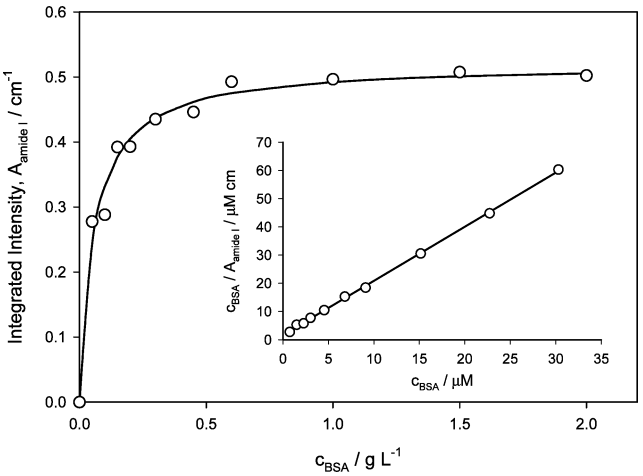

Figure 2. Dependence of the amide I integrated intensity ($A_{amide\ I}$) on the bulk equilibrium BSA concentration (c_{BSA}) at 295 K. The data was obtained from PM-IRRAS spectra of the 316LVM stainless steel surface following immersion in PBS (pH 7.4) solution containing various BSA concentrations. Symbols represent the experimental data, whereas the solid line represents the fitted Langmuir isotherm. Inset: Linearized form of the Langmuir isotherm describing the adsorption of BSA onto 316LVM stainless steel at 295 K.

estimates until the best fit was obtained. The resulting frequency position of each peak was then fixed, and only the width and intensity were allowed to vary for all subsequent fitting at lower bulk protein concentrations. This allowed for direct comparisons of the fitted peaks within each set of experimental data. On the basis of guidelines provided in the literature,[10,43,47,48] the fitted component peaks were each assigned to specific secondary structures on the basis of their position (Table 2). The integrated areas of the fitted component bands are directly proportional to the relative proportions of the secondary structure they represent, and were thus expressed as a percentage of the total amide I area.

3. Results and Discussion

3.1. Thermodynamics of BSA and Fibrinogen Adsorption. *3.1.1. PM-IRRAS Spectra.* PM-IRRAS was first applied in this research to investigate the thermodynamics of BSA and fibrinogen adsorption onto a biomedical-grade 316LVM stainless steel surface. When studying surface-adsorbed proteins using IR techniques, the spectral region of interest includes the amide I and amide II bands. These bands, which are characteristic of all proteins, arise from the different vibrational modes of the polypeptide backbone. The amide I band occurs approximately between 1600 and 1700 cm^{-1}, and represents mainly 80% of the C═O stretching vibration of the amide group coupled to approximately 10% C−N stretching and 10% in-plane N−H bending modes.[48] The amide II band represents mainly 60% N−H bending coupled to some C−N stretching (40%) of the protein's amide groups.[48] In this study, the analysis was focused on the amide I band of the PM-IRRAS spectra due to its strong, well-defined signal, in addition to the possibility of later extracting information on the secondary structures of the surface-adsorbed BSA and fibrinogen molecules.

For the spectroscopic equilibrium adsorption experiments, the stainless steel coupons were immersed in PBS (pH 7.4) solutions containing various concentrations of either BSA or fibrinogen long enough to ensure that an equilibrium state was reached (ca. 40 min). Following thorough rinsing and drying, the coupons were then analyzed using PM-IRRAS, as previously described. Figure 1 shows a set of selected PM-IRRAS spectra in the amide region of the 316LVM stainless steel surface following its immersion in PBS solutions containing increasing BSA concentrations at 295 K. The PM-IRRAS spectra indicate that the protein is indeed present on the stainless steel surface. Similar spectra were obtained following immersion of the coupons in the fibrinogen solutions at the same temperature (not shown).

3.1.2. Adsorption Isotherms. Figure 1 demonstrates that, with an increase in BSA concentration in the bulk solution, the overall intensity of the amide I band also increases, indicating progressively greater surface concentrations of BSA. This trend is shown more clearly in Figure 2, in which the curve displays a shape characteristic of a Type I adsorption isotherm. The protein surface concentration increases with an increase in bulk BSA concentration, and then levels off into a plateau at a bulk BSA concentration of ca. 0.6 g L^{-1}, indicating that saturated (monolayer) BSA coverage is reached. A similar behavior was observed with fibrinogen (Figure 3), although the saturated surface concentration was not reached in the fibrinogen bulk solution concentration range investigated. However, our measurements on the interaction of fibrinogen with the 316LVM surface using EIS[49] showed that when increasing the fibrinogen bulk solution concentration above the highest value presented in Figure 3, the corresponding fibrinogen surface coverage quickly reaches a plateau, thus confirming that the adsorption of fibrinogen on 316LVM also obeys a Type I adsorption isotherm.

The ultimate aim of these adsorption experiments was to obtain insight on the thermodynamics related to the adsorption of BSA and fibrinogen onto a 316LVM stainless steel surface using PM-IRRAS. In order to extract such information, it is necessary to model the experimental data using an adsorption isotherm. Our previous results[50] showed that the adsorption of proteins on charged metal surfaces is a reversible process characterized, however, by very slow desorption kinetics. Other studies[51,52] have also shown that the protein adsorption/desorption cycle is reversible in terms of the protein secondary structure changes. Taking the observations from references 50−52 into account, and on the basis of our previous protein adsorption studies[39,50,53−56] and studies of other research groups,[35,57−66] the Langmuir isotherm was selected to model the adsorption data obtained from the PM-IRRAS experiments.

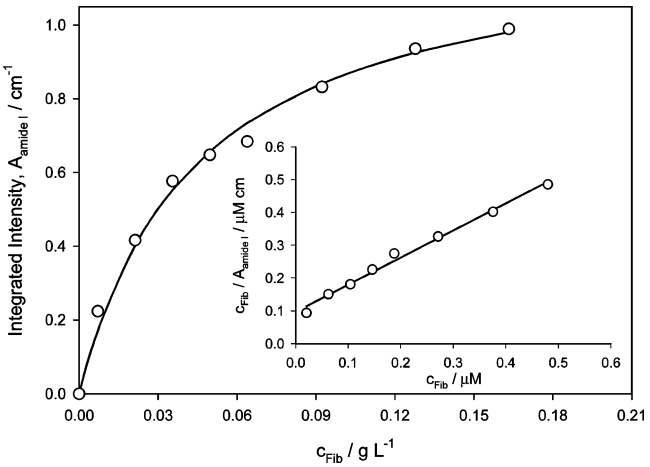

Figure 3. Dependence of the amide I integrated intensity ($A_{amide\ I}$) on the bulk equilibrium fibrinogen concentration (c_{Fib}) at 295 K. The data was obtained from PM-IRRAS spectra of the 316LVM stainless steel surface following immersion in PBS (pH 7.4) solution containing various fibrinogen concentrations. Symbols represent the experimental data, whereas the solid line represents the fitted Langmuir isotherm. Inset: Linearized form of the Langmuir isotherm describing the adsorption of fibrinogen onto 316LVM stainless steel at 295 K.

Since the area under each amide I band (integrated intensity) is proportional to the protein surface concentration, the Langmuir isotherm can be expressed as

$$A = \frac{A_{max} B_{ads} c}{1 + B_{ads} c} \quad (1)$$

where A is the integrated area of the amide I peak (cm^{-1}), A_{max} is the integrated area of the amide I peak at the maximum (saturated) protein surface concentration, c (mol L^{-1} = M) is the equilibrium concentration of the protein in the bulk solution, and the parameter B_{ads} (L mol^{-1}), known as the adsorption affinity constant, reflects the affinity of the protein toward surface adsorption sites at a constant temperature. It is possible to further rearrange eq 1 to yield a linearized form of the Langmuir isotherm:

$$\frac{c}{A} = \frac{1}{B_{ads} A_{max}} + \frac{c}{A_{max}} \quad (2)$$

Therefore, on the basis of eq 2, for the Langmuir isotherm to be considered valid for both protein systems under investigation, a plot of c/A versus concentration c should yield a straight line with parameters A_{max} and B_{ads} derived from the slope and the intercept, respectively. Indeed, the inset to Figure 2 demonstrates the linear trend (correlation coefficient $R^2 = 0.9994$) displayed by the data recorded for the adsorption of BSA onto the stainless steel surface at 295 K. For the fibrinogen adsorption experiments, a linear trend was also observed (inset to Figure 3, coefficient $R^2 = 0.9907$). As a result, the Langmuir isotherm was deemed applicable in describing the adsorption of both proteins onto the 316LVM stainless steel surface.

3.1.3. Gibbs Energy of Adsorption. As previously mentioned, the adsorption affinity constant B_{ads} can be obtained from the intercept of the linearized plot. For the experimental data presented in Figure 2, the maximum integrated intensity and adsorption affinity constant for the adsorption of BSA onto the steel surface at 295 K was found to be $A_{max,BSA} = 0.52$ and $B_{ads,BSA} = 1.15 \times 10^6$ L mol^{-1}, whereas the data in Figure 3 yielded $A_{max,Fib} = 1.21$ and $B_{ads,Fib} = 6.05 \times 10^6$ L mol^{-1} for the adsorption of fibrinogen onto the same steel surface at 295 K. Using the calculated B_{ads} values, a fundamental thermodynamic parameter, the Gibbs energy of adsorption, ΔG_{ads} (J mol^{-1}), can be calculated:

$$B_{ads} = \frac{1}{c_{solvent}} \exp\left(\frac{-\Delta G_{ads}}{RT}\right) \quad (3)$$

where $c_{solvent}$ (mol L^{-1}) is the molar concentration of the solvent, which, in this case, corresponds to water ($c_{water} = 55.5$ mol L^{-1}), R (J mol^{-1} K^{-1}) is the gas constant, and T (K) is the temperature of the system. By applying eq 3, the apparent Gibbs energy of adsorption associated with the adsorption of BSA and fibrinogen onto the 316LVM stainless steel at 295 K was calculated to be -44.1 kJ mol^{-1} and -49.0 kJ mol^{-1}, respectively. These highly negative ΔG_{ads} values indicate a highly spontaneous and strong adsorption of both BSA and fibrinogen onto the 316LVM stainless steel. The difference between the two values is due to the difference in the molar weights of the two proteins, which is in accordance with the results in the literature.[35]

Using EIS, a higher value of apparent Gibbs energy, -57.2 kJ mol^{-1}, has been reported for the adsorption of BSA on a 316L stainless steel surface at 299 K in phosphate buffer pH 7.0.[55] This Gibbs energy was calculated indirectly by measuring the corrosion rate of 316L (in the absence and presence of BSA), which could be the reason for its higher value when compared to the value in the present study. Other studies investigating the adsorption of BSA onto a platinum[35] and titanium[54] surface using cyclic voltammetry reported ΔG_{ads} values of -48.0 and -48.2 kJ mol^{-1}, respectively, in phosphate buffer pH 7.4 and at 298 K. Using EIS, our laboratory determined the apparent Gibbs energy of adsorption of BSA on a positively charged Pt electrode surface of -45.5 kJ mol^{-1} in phosphate buffer pH 7.4 at 298 K.[50]

Concerning fibrinogen adsorption, we obtained in another study using EIS a ΔG_{ads} value of -50.1 kJ mol^{-1} for the adsorption of fibrinogen onto the same 316LVM stainless steel surface at 295 K, which is in very good agreement with the value reported here. A study applying different experimental techniques reported ΔG_{ads} values ranging from -49.6 to -50.8 kJ mol^{-1} for the adsorption of fibrinogen onto a platinum surface at 298 K,[50] whereas cyclic voltammetric studies on the adsorption of fibrinogen onto a titanium surface reported ΔG_{ads} values of -39.9 kJ mol^{-1} at 295 K and -54.2 kJ mol^{-1} at 310 K.[54] From the results presented in ref 67, a ΔG_{ads} value of -52.0 kJ mol^{-1} could be calculated for the adsorption of fibrinogen on hydrophilic glass in phosphate buffer pH 7.4 at 298 K.

Therefore, although a divergence is to be expected because of the different surfaces investigated, the electrolytes used, the sensitivity of the different applied techniques, and the overall difficulty in reproducing similar experimental conditions by different research groups, the ΔG_{ads} values obtained using PM-IRRAS in the present research are comparable to the values previously reported in the literature. This demonstrates the potential of implementing the PM-IRRAS technique to investigate the equilibrium adsorption behavior of proteins and to extract the associated Gibbs energy of adsorption.

3.1.4. Surface Conformation. It is also worth noting from Figures 2 and 3 that the ratio between the A_{max} values calculated by fitting the adsorption data is $(A_{max,Fib}/A_{max,BSA})_{exp} = 2.3$. Knowing that the integrated intensity of the amide I peak (Figure 1) is proportional to the number of C═O stretching vibrations, this result suggests that the number of the fibrinogen's amino acids per unit of 316LVM surface area (which is the total number of amino acids plus the number of acidic amino acids)

is also ca. 2.3 times that achieved by the BSA's amino acids. Assuming both proteins are adsorbed on the 316LVM surface with a "side-on" orientation, and taking the dimensions of the molecules listed in the Introduction, the theoretical close-packed monolayer concentrations of each protein can be calculated to be 4.73×10^{11} molecules/cm^2 for fibrinogen versus 17.54×10^{11} molecules/cm^2 for BSA. Further, the total number of amino acids in fibrinogen is 2875, 685 of which are acidic amino acids,[68] while 585 amino acids form the serum albumin molecule, 101 of which are acidic amino acids.[8] Taking into account the above theoretical surface concentration values of the proteins and the total number of amino acids contributing to the amide I response (i.e., the total number of C═O stretches), the theoretical ratio between $A_{max,Fib}$ and $A_{max,BSA}$ is calculated to be 1.4. This value is lower than the ratio between the corresponding A_{max} values obtained from the experimental data in Figures 2 and 3, $(A_{max,Fib}/A_{max,BSA})_{exp} = 2.3$, and could be explained in the following way.

Our analysis of the BSA amide I band (Section 3.2.2, Figure 5) shows that, at saturated BSA coverages, a significant degree of secondary structure of the molecule is lost upon adsorption on the 316LVM surface. This indicates that the adsorbed BSA molecule most likely unfolds on the 316LVM surface which, in turn, results in a lower surface concentration of the protein when compared to the above theoretical value calculated on the basis of the dimensions of native (nondenatured) BSA. Furthermore, the analysis of the fibrinogen amide I band suggests that the protein adopts a "bent" conformation upon adsorption (as discussed in further detail in Section 3.2.3), thus lowering the projected length of the molecule below the value for the fully extended molecule (45 nm). Such a surface conformation would, in turn, accommodate a larger number of fibrinogen molecules adsorbed on the unit area of the 316LVM surface than if these were adsorbed in a completely flat (extended) configuration. Taking into account these two opposing conformation changes occurring upon adsorption of BSA and fibrinogen on the 316LVM surface, it is now obvious why $(A_{max,Fib}/A_{max,BSA})_{exp}$ is greater than $(A_{max,Fib}/A_{max,BSA})_{calc}$.

Our observation can further be substantiated by findings reported by previous studies that have implemented atomic force microscopy to characterize the structure of surface-adsorbed fibrinogen.[62,69−71] High-resolution images of fibrinogen adsorbed on atomically flat mica and highly oriented pyrolytic graphite (HOPG) (which serve as model hydrophilic and hydrophobic surfaces, respectively) indicate that the surface wettability influences fibrinogen's adsorbed conformation. Marchin et al.[70] observed that most fibrinogen molecules adsorbed on the hydrophobic HOPG surface were characterized by a trinodular morphology, whereas the majority of fibrinogen molecules adsorbed on the hydrophilic mica surface appeared more compact and globular, thus suggesting a "bent" conformation. Analogous observations were made by Gettens et al.[62] and Ta et al.,[71] who also investigated the adsorption of fibrinogen on HOPG and mica, as well as by Lin et al.,[69] who studied the adsorption of fibrinogen on CH_3- and OH-terminated self-assembled monolayers (SAMs). On the basis of these findings, adsorption models have been proposed where fibrinogen is believed to adsorb onto hydrophobic surfaces through its hydrophobic D and E domains, leaving the hydrophilic αC domains free in solution to interact with other fibrinogen molecules. Conversely, it is hypothesized that the αC domains fold under the fibrinogen molecule when it adsorbs onto hydrophilic surfaces, thereby producing the compact, globular conformation.

Therefore, since the 316LVM stainless steel used in this research corresponds to a hydrophilic surface, and taking into account the PM-IRRAS results discussed above and later in the text (Section 3.2.3), it is reasonable to presume that fibrinogen is indeed adsorbed on the surface in a "bent" conformation with the αC domains folded under the molecule, while the adsorbed BSA molecule unfolds to a certain extent.

3.2. Secondary Structure Changes of Adsorbed BSA and Fibrinogen. The secondary structure of proteins plays one of the major roles in determining the degree of their activity in specific physiological processes. For example, deviations in the original (native) secondary structure of enzymes may lead to their complete deactivation, or loss of their selectivity, and the same could be said for surface-immobilized antibodies/antigens. Consequently, deviations in the native secondary structure of serum albumin and fibrinogen, as a (possible) result of their interaction with the biomaterial's surface, may lead to the loss of their physiological activity/selectivity, increased corrosion of metallic biomaterials, irreversible fouling of the biomaterial's surface, an increase in its thrombogenicity, and so forth. Therefore, it is of major importance to investigate the secondary structure of serum albumin and fibrinogen adsorbed on the biomaterial's surface so as to determine the extent of loss in their secondary structure with respect to their respective native states.

3.2.1. Deconvolution of PM-IRRAS Spectra. In order to obtain insight on the secondary structure of BSA and fibrinogen adsorbed onto the 316LVM stainless steel surface, the amide I bands of the PM-IRRAS spectra were analyzed. The conformational sensitivity of the amide I band can be mainly attributed to hydrogen bonding and coupling between transition dipole moments, which leads to splitting of the band.[72] The extent of this splitting depends on the orientation and distance of the dipoles, and therefore provides information on the geometrical arrangements of the peptide groups in the protein's polypeptide chain. As a result, the amide I band observed in the spectrum is actually a complex composite consisting of various overlapping component bands that each represent different secondary structures. The most widely implemented approach to extracting this encoded structural information consists of an iterative least-squares curve-fitting technique, already explained in Section 2.4.

Prior to presenting the results obtained from the conformational study, it is important to have knowledge of the secondary structure of BSA and fibrinogen in their native states. Spectroscopic studies in the literature[10,51,52,73,74] have reported the secondary structure distribution of BSA in solution to be 53−60% α-helix, 5−22% β-sheet, 3−13% β-turns, and approximately 16−30% random coils (Scheme 1). Studies investigating the secondary structure of fibrinogen[45,75−79] have reported the distribution of fibrinogen's secondary structural elements as 30−37% α-helix, 21−30% β-sheet, 12−19% β-turns, and 16−39% random structures (Scheme 2). Therefore, BSA can be predominantly characterized by its high α-helical content, while fibrinogen's secondary structure can be predominantly characterized by both the α-helical and β-sheet content.

As a representative example of the conformational analysis performed in this research, the experimental PM-IRRAS spectra recorded for the adsorption of BSA onto the 316LVM stainless steel surface were selected for discussion. Figure 4A shows the amide I band fitted with its resulting component peaks. Secondary structures were assigned to each fitted component peak based on their position (Table 2), and their content was expressed as a percentage of the total experimental amide I band area. Figure 4A shows that the sum of the fitted underlying

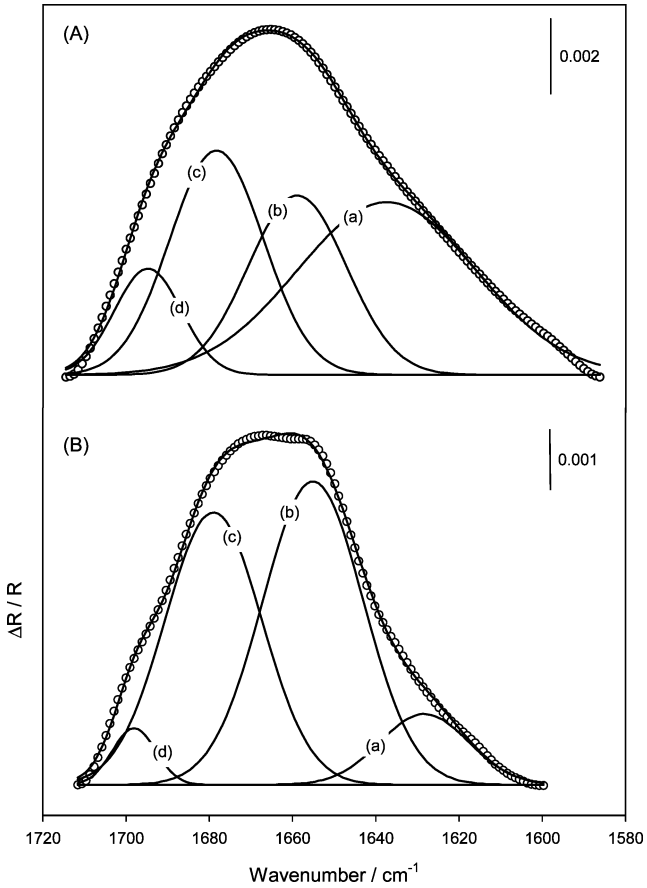

Figure 4. Amide I band fitted with its underlying component bands. Symbols (○) represent the experimental PM-IRRAS spectrum of the 316LVM stainless steel surface following immersion in a PBS (pH 7.4) solution containing (A) 2 g L^{-1} and (B) 0.15 g L^{-1} of BSA at 295K. The sum of the component bands yields the overall simulated amide I band (dark line passing through the symbols), which fits the experimental band contour well. Secondary structures of the component bands were assigned as follows: (a) β-sheet, (b) α-helix, (c) β-turns, and (d) β-turns and CO_{COOH} stretching modes of −COOH groups in acidic amino acids (Asp and Glu).

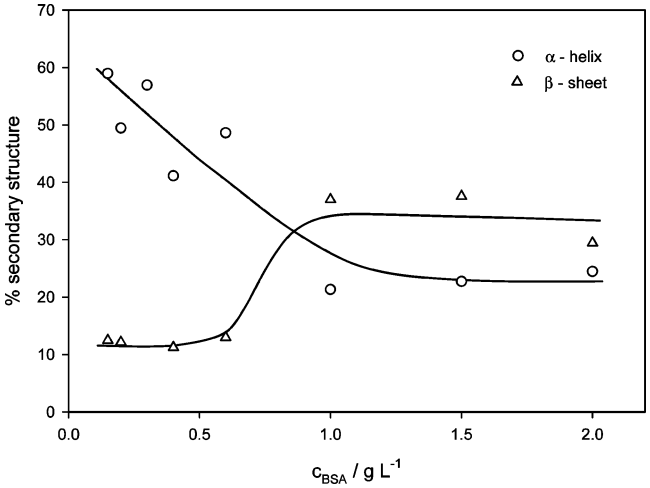

Figure 5. Changes in BSA's (○) α-helix and (Δ) β-sheet content as a function of protein concentration in the bulk solution, obtained from fitting the experimental PM-IRRAS spectra of BSA adsorbed on the 316LVM stainless steel surface following immersion in a PBS (pH 7.4) solution at 295 K. Solid lines are included only as a visual aid, and do not represent efforts to model the experimental data.

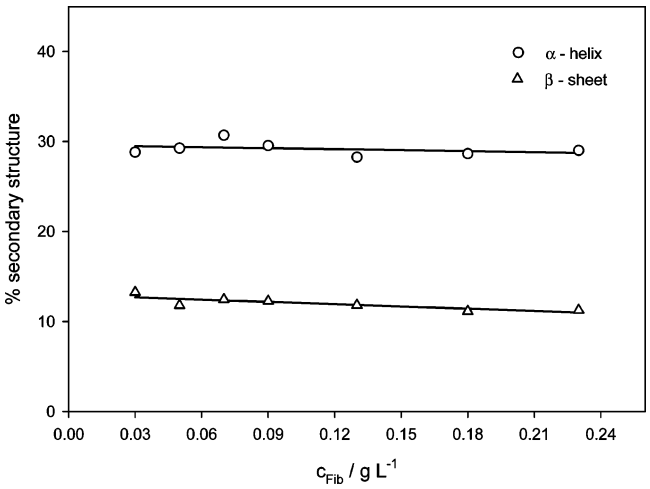

Figure 6. Changes in fibrinogen's (○) α-helix and (Δ) β-sheet content as a function of bulk protein concentration, obtained from fitting the experimental PM-IRRAS spectra of fibrinogen adsorbed on the 316LVM stainless steel surface following immersion in a PBS (pH 7.4) solution at 295 K. Solid lines are included only as a visual aid, and do not represent efforts to model the experimental data.

component bands yields a simulated amide I band (solid line) that is in very good agreement with the experimental band contour (symbols). A good agreement was observed between the simulated and experimental amide I bands even for the spectra recorded at lower protein concentrations in the bulk solution (Figure 4B). When analyzing the experimental PM-IRRAS spectra associated with the adsorption of fibrinogen onto the 316LVM stainless steel, the same fitting methodology was implemented, and a very good agreement between the simulated and experimental data was also obtained.

Since α-helix and β-sheet are the two dominating secondary structures in BSA and fibrinogen, this study focused on the conformational changes of the two proteins by investigating the changes of their α-helix and β-sheet secondary structures. In addition, most studies investigating the conformational changes of these two proteins in the literature have also focused on the α-helix and β-sheet secondary structures, which allowed us to compare our results to the literature results. Figures 5 and 6 show the respective changes in the α-helix and β-sheet contents of BSA and fibrinogen as a function of bulk protein concentration at 295 K, as obtained from fitting the experimental PM-IRRAS spectra.

3.2.2. Changes in the Secondary Structure of Adsorbed BSA. The results presented in Figure 5 indicate that the α-helix content of BSA adsorbed onto the 316LVM stainless steel surface gradually decreases, from ca. 59% to ca. 25%, as the concentration of the protein in the bulk solution increases. This α-helix loss seems to be accompanied by a gradual increase in the β-sheet content from ca. 12% to 35%. This implies that, with an increase in the surface and equilibrium bulk concentration of BSA, a part of the α-helix structure transforms into the β-sheet structure. At a bulk BSA concentration of 2 g L^{-1}, the protein's secondary structure is defined by an almost equal percentage of the α-helix and β-sheet content. Therefore, the results in Figure 5 clearly demonstrate that, with respect to the native state, a significant portion of BSA's secondary structure is lost upon its adsorption to the 316LVM surface (a ca. 58% decrease in the α-helix content and >100% increase in the β-sheet content). This, in turn, indicates unfolding of the protein upon adsorption.

Similar findings were reported by Roach et al.,[5] who found that BSA lost a large percentage of its α-helical content, while a concurrent increase in the β-sheet component was observed when the protein adsorbed on a SAM-modified gold-coated glass

surface. Ishiguro et al.[80] also reported that BSA adsorbed onto a solid poly tris(trimethylsiloxy)silylstyrene surface had a smaller α-helix content than that of dissolved BSA, whereas the content of β-structures was larger. To the best of our knowledge, no data on the investigation of the secondary structure of BSA adsorbed on stainless steel is available in the literature, which prevents independent direct verification of our results. Nevertheless, the significant reduction in the α-helical component of BSA following its adsorption onto the stainless steel observed in this research is consistent with several studies that have also reported a lower α-helical content for BSA adsorbed on some other materials, including silica,[51,52,81] polystyrene particles,[52] hematite,[82] and ceramic particles.[10]

Further, comparison of the results presented in Figures 2 and 5 shows that lower α-helix and higher β-sheet content is obtained with increasing concentrations of BSA in the bulk solution, i.e., increasing surface coverage. This may indicate that, at higher surface coverages, lateral interactions between the adsorbed BSA molecules induce more extensive structural changes in the protein. Furthermore, the β-sheet is a more stable secondary structure than the α-helix, which would explain the favored β-sheet increase from a thermodynamic reasoning, too. Similar conclusions were reported by Ishiguro et al.,[80] who noted that the conformational changes of BSA adsorbed onto poly tris(trimethylsiloxy)silylstyrene could be described solely as a function of adsorption amount. Results by Koutsoukos et al.[82] also indicated that albumin molecules arriving first at a hematite surface underwent minimal structural changes, whereas molecules arriving later underwent conformational changes that were most likely attributable to lateral interactions.

3.2.3. Changes in the Secondary Structure of Adsorbed Fibrinogen. In the case of fibrinogen, the results presented in Figure 6 indicate that fibrinogen adsorbed onto the 316LVM stainless steel surface has a β-sheet content that appears to be relatively constant at ca. 12%. However, compared to the β-sheet content in native fibrinogen (21−30%),[45,75−77] the results in Figure 6 demonstrate that the protein losses a significant amount of the β-sheet content upon adsorption. The β-sheet value in Figure 6 is also lower than that reported by both Azpiazu et al. (30%)[75] and Yongli et al.[76] (21%). Since the former study determined that most of fibrinogen's β-sheet content is present in the two globular D domains (Scheme 2), the lower β-sheet content obtained in the present research could indicate that a certain degree of unfolding of fibrinogen's D domains occurs upon adsorption to the stainless steel. Tunc et al.[46] also observed a decrease in the β-sheet content of fibrinogen upon its adsorption to silicon wafers. In another study,[10] a similar decrease in the β-sheet content was also reported for fibrinogen adsorbed onto alumina and hydroxyapatite particles.

Additionally, Figure 6 also indicates that fibrinogen adsorbed onto the 316LVM stainless steel surface appears to have an α-helical content of ca. 30% that is relatively constant for the investigated concentration range. The fact that this value is in the lower range of those reported in the literature (30−37%) could indicate some minor structural rearrangements of fibrinogen's coiled coils and/or unfolding of the protein's globular domains upon adsorption to the 316LVM stainless steel surface, since it has been determined that the D domains of the fibrinogen molecule also contains some helical structure (ca. 35%).[75] Other studies have also reported adsorption-induced conformational changes in the α-helical content of fibrinogen. Yongli et al.[76] reported a gradual decrease in the α-helix content of fibrinogen (from 35.4% to 15.1%) during adsorption, rinsing, and desorption from TiO_2 particles. Brandes et al.[10] noted a similar decrease in the α-helical content of fibrinogen upon adsorption onto alumina and hydroxyapatite ceramic particles. Chan and Brash[83] reported that the α-helix content of fibrinogen was reduced to approximately half its value in the native state after desorption of the protein from glass.

Scheme 3. Effect of Adsorbed Fibrinogen's Configuration on the α-Helix Signal Observed in the Spectrum, as Determined by the Surface Selection Rule of the PM-IRRAS Technique[a]

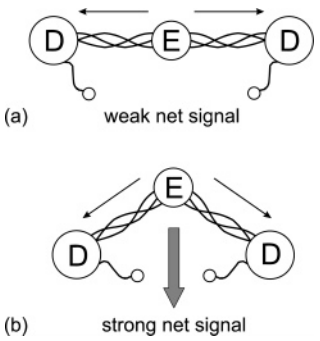

[a] In (a), only a weak net signal would be observed in the spectrum if fibrinogen were adsorbed in a completely flat configuration, since the dipole moments of the coiled coils would cancel. In (b), a stronger net signal would be observed in the spectrum if fibrinogen were adsorbed in a bent-type configuration.

Since ca. 70% of fibrinogen's total α-helical content is attributed to the coiled coils that connect the protein's outer D domains to the central E domain[84] (Scheme 2), it can be assumed that the α-helix signal observed in the PM-IRRAS spectra arises mainly from contributions of the coiled coils. Consequently, the observed reduction in the α-helical content of surface-adsorbed fibrinogen (Figure 6) relative to the content of native fibrinogen could also be partially attributed to a decrease in the angle between the protein's coiled coils. According to the surface selection rule of the PM-IRRAS technique, only bonds having a transition dipole moment component perpendicular to the surface will be observed in the recorded spectrum, and therefore the technique may be applied to infer the molecular orientation of the surface-adsorbed fibrinogen molecules. Therefore, if the fibrinogen molecules were adsorbed in a completely flat configuration on the stainless steel surface (Scheme 3a), only a weak α-helix signal (coming from other domains of the protein, which contain ca. 30% of the total α-helical content) would be detected in the spectrum because the dipole moments from the pair of coiled coils would cancel. On the other hand, a net α-helix signal would be observed in the spectrum if the fibrinogen molecules were adsorbed on the surface in any type of bent configuration (Scheme 3b).

On the basis of this reasoning, it can be deduced from the results in Figure 6 that the fibrinogen molecules adsorb in a "bent" configuration on the 316LVM surface. This conclusion is in agreement with the literature[62,69−71] and is also supported by the results discussed in Section 3.1.4 from which it was determined that the $A_{max,Fib}/A_{max,BSA}$ ratio is higher than that calculated on the basis of the dimensions of the two proteins in a native state.

3.2.4. Adsorption Driving Force. The results obtained in this research show that BSA and fibrinogen change secondary structure and conformation to a certain extent upon adsorbing to the 316LVM stainless steel surface. Thermodynamic investigations of various proteins have found protein adsorption onto solid surfaces to be a spontaneous process characterized by negative values of the apparent Gibbs energy of adsorption. In this research, this has also been shown to be the case for BSA and fibrinogen adsorption onto a 316LVM stainless steel surface

(Section 3.1.3). Our and other studies have found the entropy gain to be the primary contribution to the overall Gibbs energy of adsorption, thus indicating that protein adsorption is often an entropically driven process.[39,49,50,54,59] Therefore, changes in the secondary structure of BSA and fibrinogen observed in the present study would consequently cause an increase in the rotational mobility along the polypeptide chain, and thus lead to larger conformational entropy that would contribute to the overall entropy gain that drives the adsorption process.[85] It is worth mentioning that another factor that also contributes to an entropy gain is the dehydration of the protein and stainless steel surface.[86] Adsorption of BSA and fibrinogen may displace highly ordered water molecules that are aligned at the charged stainless steel surface, thus increasing the disorder at the molecular level and leading to an additional entropy gain.[87]

4. Conclusions

The PM-IRRAS results show that BSA and fibrinogen adsorb spontaneously and strongly on the 316LVM stainless steel surface, as evidenced by the large, negative apparent Gibbs energy values obtained at the investigated temperature. Both proteins change secondary structure upon adsorption.

The α-helix content of BSA adsorbed onto the 316LVM stainless steel surface gradually decreases as the concentration of the protein in the bulk solution increases, accompanied by a gradual increase in the β-sheet content. This suggests that at higher surface concentrations, lateral interactions between the BSA molecules induce more extensive secondary structure changes.

The secondary structure of fibrinogen adsorbed onto the 316LVM surface is not influenced by lateral interactions between the adsorbed fibrinogen molecules, as evidenced by a surface-concentration independent α-helix and β-sheet content. However, while the α-helix content of the adsorbed fibrinogen is only slightly lower than that reported for native protein, its β-sheet content decreases by ca. 50% upon adsorption. This indicates a small degree of structural rearrangement of fibrinogen's coiled coils, but large structural rearrangements of the protein's globular domains upon its adsorption to the stainless steel surface, respectively. The PM-IRRAS results also indicate that the fibrinogen molecule adsorbs in a "bent" configuration on the 316LVM surface.

It was demonstrated that the PM-IRRAS technique is a viable tool for investigating the adsorption behavior of proteins at biomaterial surfaces, as well as for obtaining information on the adsorption-induced changes in the secondary structure of proteins. This is particularly advantageous, since a better understanding of these adsorption-induced conformational and structural changes is crucial for the future development of more biocompatible materials.

Acknowledgment. Grateful acknowledgment is made to the Natural Science and Engineering Research Council of Canada and the Centre for Biorecognition and Biosensors at McGill University for support of this research.

References and Notes

(1) Wahlgren, M.; Arnebrant, T. *Trends Biotechnol.* **1991**, *9*, 201−8.
(2) Martins, M. C. L.; Wang, D.; Ji, J.; Feng, L.; Barbosa, M. A. *Biomaterials* **2003**, *24*, 2067−76.
(3) Xiang, Z.; Spector, M. *Encyclopedia of Medical Devices and Instrumentation*, 2nd ed.; John Wiley & Sons, Inc.: New York, 2006.
(4) Mikhaylova, Y.; Dutschk, V.; Muller, M.; Grundke, K.; Eichhorn, K. J.; Voit, B. *Colloids Surf., A: Physicochem. Eng. Aspects* **2007**, *297*, 19−29.
(5) Roach, P.; Farrar, D.; Perry, C. C. *J. Am. Chem. Soc.* **2005**, *127*, 8168−73.
(6) Liu, F. Y.; Zhou, M. Y.; Zhang, F. *Appl. Radiat. Isot.* **1998**, *49*, 67−72.
(7) Spector, A. A. *Methods Enzymol.* **1986**, *128*, 320−39.
(8) Sugio, S.; Kashima, A.; Mochizuki, S.; Noda, M.; Kobayashi, K. *Protein Eng.* **1999**, *12*, 439−46.
(9) Brown, J. H.; Volkmann, N.; Jun, G.; Henschen-Edman, A. H.; Cohen, C. *Proc. Natl. Acad. Sci. U.S.A.* **2000**, *97*, 85−90.
(10) Brandes, N.; Welzel, P. B.; Werner, C.; Kroh, L. W. *J. Colloid Interface Sci.* **2006**, *299*, 56−69.
(11) Mosesson, M. W.; Siebenlist, K. R.; Meh, D. A. *Fibrinogen* **2001**, *936*, 11−30.
(12) Feng, L.; Andrade, J. D. *Proteins at Interfaces II: Fundamentals and Applications*; Horbett, T. A., Brash, J. L., Eds.; American Chemical Society: Washington, DC, 1995; Chapter 5.
(13) Fuss, C.; Palmaz, J. C.; Sprague, E. A. *J. Vasc. Interv. Radiol.* **2001**, *12*, 677−82.
(14) Bailly, A. L.; Laurent, A.; Lu, H.; Elalami, I.; Jacob, P.; Mundler, O.; Merland, J. J.; Lautier, A.; Soria, J.; Soria, C. *J. Biomed. Mater. Res.* **1996**, *30*, 101−08.
(15) Chinn, J. A.; Horbett, T. A.; Ratner, B. D. *Thromb. Haemostasis* **1991**, *65*, 608−17.
(16) Stevens, P. W.; Hansberry, M. R.; Kelso, D. M. *Anal. Biochem.* **1995**, *225*, 197−205.
(17) Weber, N.; Wendel, H. P.; Ziemer, G. *Biomaterials* **2002**, *23*, 429−39.
(18) Bentaleb, A.; Abele, A.; Haikel, Y.; Schaaf, P.; Voegel, J. C. *Langmuir* **1999**, *15*, 4930−33.
(19) Lhoest, J. B.; Detrait, E.; van den Bosch de Aguilar, P.; Bertrand, P. *J. Biomed. Mater. Res.* **1998**, *41*, 95−103.
(20) Wagner, M. S.; Horbett, T. A.; Castner, D. G. *Biomaterials* **2003**, *24*, 1897−908.
(21) Armstrong, J.; Salacinski, H. J.; Mu, Q. S.; Seifalian, A. M.; Peel, L.; Freeman, N.; Holt, C. M.; Lu, J. R. *J. Phys.: Condens. Matter* **2004**, *16*, S2483−91.
(22) Hook, F.; Voros, J.; Rodahl, M.; Kurrat, R.; Boni, P.; Ramsden, J. J.; Textor, M.; Spencer, N. D.; Tengvall, P.; Gold, J.; Kasemo, B. *Colloids Surf., B: Biointerfaces* **2002**, *24*, 155−70.
(23) Malmsten, M.; Lessen, B. *Proteins Interfaces II* **1995**, *602*, 228−38.
(24) Seitz, R.; Brings, R.; Geiger, R. *Appl. Surf. Sci.* **2005**, *252*, 154−7.
(25) Toscano, A.; Santore, M. M. *Langmuir* **2006**, *22*, 2588−97.
(26) Mollmann, S. H.; Jorgensen, L.; Bukrinsky, J. T.; Elofsson, U.; Norde, W.; Frokjaer, S. *Eur. J. Pharm. Sci.* **2006**, *27*, 194−204.
(27) Ngankam, A. P.; Mao, G. Z.; Van Tassel, P. R. *Langmuir* **2004**, *20*, 3362−70.
(28) Kurrat, R.; Walivaara, B.; Marti, A.; Textor, M.; Tengvall, P.; Ramsden, J. J.; Spencer, N. D. *Colloids Surf., B: Biointerfaces* **1998**, *11*, 187−201.
(29) Wegner, G. J.; Wark, A. W.; Lee, H. J.; Codner, E.; Saeki, T.; Fang, S. P.; Corn, R. M. *Anal. Chem.* **2004**, *76*, 5677−84.
(30) Chapman, R. G.; Ostuni, E.; Yan, L.; Whitesides, G. M. *Langmuir* **2000**, *16*, 6927−36.
(31) Evans-Nguyen, K. M.; Fuierer, R. R.; Fitchett, B. D.; Tolles, L. R.; Conboy, J. C.; Schoenfisch, M. H. *Langmuir* **2006**, *22*, 5115−21.
(32) Huang, Y. W.; Gupta, V. K. *J. Chem. Phys.* **2004**, *121*, 2264−71.
(33) Forciniti, D.; Hamilton, W. A. *J. Colloid Interface Sci.* **2005**, *285*, 458−68.
(34) Petrash, S.; Cregger, T.; Zhao, B.; Pokidysheva, E.; Foster, M. D.; Brittain, W. J.; Sevastianov, V.; Majkrzak, C. F. *Langmuir* **2001**, *17*, 7645−51.
(35) Cosman, N. P.; Roscoe, S. G. *Langmuir* **2004**, *20*, 1711−20.
(36) Wright, J. E. I.; Cosman, N. P.; Fatih, K.; Omanovic, S.; Roscoe, S. G. *J. Electroanal. Chem.* **2004**, *564*, 185−97.
(37) Stadler, H.; Mondon, M.; Ziegler, C. *Anal. Bioanal. Chem.* **2003**, *375*, 53−61.
(38) Hemmersam, A. G.; Foss, M.; Chevallier, J.; Besenbacher, F. *Colloids Surf., B: Biointerfaces* **2005**, *43*, 208−15.
(39) Omanovic, S.; Roscoe, S. G. *J. Colloid Interface Sci.* **2000**, *227*, 452−60.
(40) Martins, M. C. L.; Fonseca, C.; Barbosa, M. A.; Ratner, B. D. *Biomaterials* **2003**, *24*, 3697−706.
(41) Chen, H.; Brook, M. A.; Chen, Y.; Sheardown, H. *J. Biomater. Sci., Polym. Ed.* **2005**, *16*, 531−48.

(42) Wagner, M. S.; Castner, D. G. *Appl. Surf. Sci.* **2004**, *231*−*2*, 366−76.
(43) Schwinte, P.; Voegel, J. C.; Picart, C.; Haikel, Y.; Schaaf, P.; Szalontai, B. *J. Phys. Chem. B* **2001**, *105*, 11906−16.
(44) Chen, Y. L.; Mao, H. B.; Zhang, X. F.; Gong, Y. D.; Zhao, N. M. *Int. J. Biol. Macromol.* **1999**, *26*, 129−34.
(45) Schwinte, P.; Voegel, J. C.; Picart, C.; Haikel, Y.; Schaaf, P.; Szalontai, B. *J. Phys. Chem. B* **2001**, *105*, 11906−16.
(46) Tunc, S.; Maitz, M. F.; Steiner, G.; Vazquez, L.; Pham, M. T.; Salzer, R. *Colloids Surf., B: Biointerfaces* **2005**, *42*, 219−25.
(47) Chittur, K. K. *Biomaterials* **1998**, *19*, 357−69.
(48) Stuart, B. *Infrared Spectroscopy: Fundamentals and Applications*; John Wiley & Sons, Inc.: Chichester, West Sussex, England, 2004; Chapter 7.
(49) Desroches, M. J. Electrochemical and PM-IRRAS studies of the interaction of plasma protein fibrinogen with a biomedical-grade 316LVM stainless steel surface. Ph.D. Thesis/Dissertation, 2007.
(50) Pyshnov, E.; Farcas, M.; Cosman, N.; Roscoe, S. G.; Omanovic, S. *Eur. Cells Mater.* **2004**, *7* (Suppl. 1), 80.
(51) Giacomelli, C. E.; Norde, W. *J. Colloid Interface Sci.* **2001**, *233*, 234−40.
(52) Norde, W.; Giacomelli, C. E. *J. Biotechnol.* **2000**, *79*, 259−68.
(53) Cabilio, N. R.; Omanovic, S.; Roscoe, S. G. *Langmuir* **2000**, *16*, 8480−88.
(54) Jackson, D. R.; Omanovic, S.; Roscoe, S. G. *Langmuir* **2000**, *16*, 5449−57.
(55) Omanovic, S.; Roscoe, S. G. *Langmuir* **1999**, *15*, 8315−21.
(56) Omanovic, S.; Roscoe, S. G. *Electrochem. Solid State Lett.* **2005**, *8*, E12−E15.
(57) Brosseau, C. L.; Maurice, M. S.; Bearne, S. L.; Roscoe, S. G. *Electrochim. Acta* **2005**, *50*, 1289−97.
(58) Cosman, N. P.; Roscoe, S. G. *Anal. Chem.* **2004**, *76*, 5945−52.
(59) Cosman, N. P.; Fatih, K.; Roscoe, S. G. *J. Electroanal. Chem.* **2005**, *574*, 261−71.
(60) Curry, S.; Mandelkow, H.; Brick, P.; Franks, N. *Nat. Struct. Biol.* **1998**, *5*, 827−35.
(61) Fukuzaki, S.; Urano, H.; Nagata, K. *J. Ferment. Bioeng.* **1995**, *80*, 6−11.
(62) Gettens, R. T. T.; Bai, Z. J.; Gilbert, J. L. *J. Biomed. Mater. Res., Part A* **2005**, *72*, 246−57.
(63) Sakiyama, T.; Tanino, K.; Urakawa, M.; Imamura, K.; Takahashi, T.; Nagai, T.; Nakanishi, K. *J. Biosci. Bioeng.* **1999**, *88*, 536−41.
(64) Bajpai, A. K.; Mishra, D. D. *J. Appl. Polym. Sci.* **2006**, *102*, 1341−55.
(65) Brash, J. L.; Tenhove, P. *J. Biomater. Sci., Polym. Ed.* **1993**, *4*, 591−99.
(66) Klinger, A.; Steinberg, D.; Kohavi, D.; Sela, M. N. *J. Biomed. Mater. Res.* **1997**, *36*, 387−92.
(67) Leduc, C.; Tenhove, P.; Park, S.; Vroman, L.; Brash, J.; Leonard, E. F. *J. Biomater. Sci., Polym. Ed.* **1995**, *7*, 531−38.
(68) Triantaphyllopoulos, E.; Triantaphyllopoulos, D. C. *Biochem. J.* **1967**, *105*, 393.
(69) Lin, Y.; Wang, J.; Wan, L. J.; Fang, X. H. *Ultramicroscopy* **2005**, *105*, 129−36.
(70) Marchin, K. L.; Berrie, C. L. *Langmuir* **2003**, *19*, 9883−8.
(71) Ta, T. C.; Sykes, M. T.; McDermott, M. T. *Langmuir* **1998**, *14*, 2435−43.
(72) Surewicz, W. K.; Mantsch, H. H.; Chapman, D. *Biochemistry* **1993**, *32*, 389−94.
(73) Rawel, H. M.; Rohn, S.; Kruse, H. P.; Kroll, J. *Food Chem.* **2002**, *78*, 443−55.
(74) Kossovsky, N.; Nguyen, A.; Sukiassians, K.; Festekjian, A.; Gelman, A.; Sponsler, E. *J. Colloid Interface Sci.* **1994**, *166*, 350−5.
(75) Azpiazu, I.; Chapman, D. *Biochim. Biophys. Acta* **1992**, *1119*, 268−74.
(76) Yongli, C.; Xiufang, Z.; Yandao, G.; Nanming, Z.; Tingying, Z.; Xinqui, S. *J. Colloid Interface Sci.* **1999**, *214*, 38−45.
(77) Soderquist, M. E.; Walton, A. G. *J. Colloid Interface Sci.* **1980**, *75*, 386−97.
(78) Budzynsk, A. Z. *Biochim. Biophys. Acta* **1971**, *229*, 663.
(79) Marx, J.; Hudryclergeon, G.; Capetantonini, F.; Bernard, L. *Biochim. Biophys. Acta* **1979**, *578*, 107−15.
(80) Ishiguro, R.; Yokoyama, Y.; Maeda, H.; Shimamura, A.; Kameyama, K.; Hiramatsu, K. *J. Colloid Interface Sci.* **2005**, *290*, 91−101.
(81) Kondo, A.; Fukuda, H. *J. Colloid Interface Sci.* **1998**, *198*, 34−41.
(82) Koutsoukos, P. G.; Norde, W.; Lyklema, J. *J. Colloid Interface Sci.* **1983**, *95*, 385−97.
(83) Chan, B. M. C.; Brash, J. L. *J. Colloid Interface Sci.* **1981**, *84*, 263−5.
(84) Doolittle, R. F.; Goldbaum, D. M.; Doolittle, L. R. *J. Mol. Biol.* **1978**, *120*, 311−25.
(85) Norde, W.; Lyklema, J. *J. Colloid Interface Sci.* **1978**, *66*, 295−302.
(86) Nadarajah, A.; Lu, C. F.; Chittur, K. K. *Proteins at Interfaces II: Fundamentals and Applications*; Horbett, T. A., Brash, J. L., Eds.; American Chemical Society: Washington, DC, 1995; Chapter 13.
(87) Norde, W. *Adv. Colloid Interface Sci.* **1986**, *25*, 267−340.

BM070289D